RSC Advances

ROYAL SOCIETY OF CHEMISTRY

www.rsc.org/advances

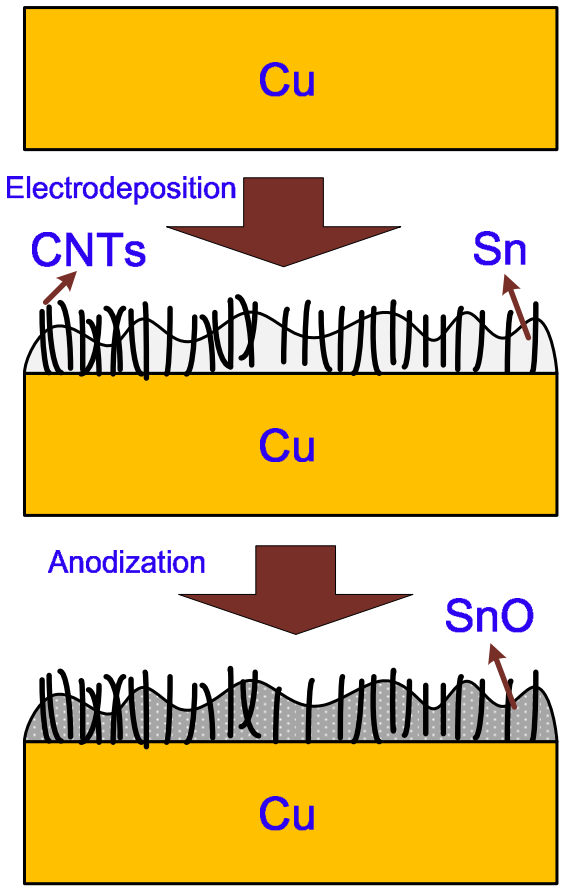

Schematic representation of the experimental procedure

In this article, ANSO@CNTs anode material was prepared with composite electrodeposition and anodicoxidation, as shown in this picture. The good electronic conductivity and mechanical properties can be guaranteed by introducing CNTs. The porous structure can facilitate liquid electrolyte diffusion into the active materials. Therefore, it could be expected that the ANSO@CNTs anode material possesses perfect cycling performance and good rate capability.

Advanced amorphous nanoporous stannous oxide composite with carbon nanotubes as anode materials for lithium-ion batteries

Wenjuan Jiang,[a] Weiyao Zeng,[a] Zengsheng Ma, [a*] Yong Pan,[a] Jianguo Lin, [a*] Chunsheng Lu[b]

[a] Key Laboratory of Low Dimensional Materials and Application Technology of Ministry of Education, and School of Materials Science and Engineering, Xiangtan University, Xiangtan 411105, Hunan, China

[b] Department of Mechanical Engineering, Curtin University, Perth, WA 6845, Australia

Abstract

An amorphous nanoporous stannous oxide (ANSO) composite with carbon nanotubes (CNTs) electrode material is synthesized by electrodeposition and anodicoxidation methods. The ANSO@CNTs as an anode material for lithium-ion batteries exhibits a high reversible specific capacity, stable cyclability and good rate capability. The first discharge capacity is as high as 1895.3 mAh g^{-1} with a reversible capacity of 1608.2 mAh g^{-1} at the current density of 100 mA g^{-1}. Furthermore, an electrochemical performance with high reversible capacity and enhanced rate capability can be found due to the highly uniform distribution and superior electrochemical and mechanical performances of CNTs. The preparation approach of ANSO@CNTs anode material reported in this paper may be applied to large-scale production of anode materials for lithium-ion batteries with high performance.

Keywords: Tin oxide, Carbon nanotube, Anodicoxidation, Anode material, Lithium-ion battery

Corresponding author: Key Laboratory of Low Dimensional Materials & Application Technology, Xiangtan University, Hunan 411105, China. Tel.: +86-731-58293577; fax: +86-731-58293577;
* zsma@xtu.edu.cn
* lin_j_g@xtu.edu.cn

1. Introduction

With the demand for high energy density, high power density, good safety performance, long life cycle, and low pollution etc., lithium-ion batteries are used as an ideal power storage device.[1-3] The anode material has a significant impact on specific capacity and cyclability as an important part of lithium-ion batteries. Graphite is the commonly used as the anode material with a theoretical specific capacity of 372 mAh g^{-1}. So far, the specific capacity of carbon anode material has been close to the theoretical specific capacity, so it is unlikely to further improve the lithium storage properties.

Tin oxide (TO) is a very promising anode material with high performances.[4] Its theoretical specific capacity is 990 mAh g^{-1} almost three times that of carbon materials, attracting the extensive attention of scientists from all over the world. Idota et al. have reported that amorphous stannous oxide possess low intercalation potential and stable cyclability, and the reversible specific capacity can reach 600 mAh g^{-1}.[5] Though the first discharge capacity of these anode materials is high, TO suffers from severe capacity fading during cycling because of the large volume deformation during the charge-discharge process.[6, 7]

There are a large number of pores in the mesoporous materials, which can probably relieve the huge volume deformation during the charge-discharge processes. Shiva et al. prepared the porous SnO_2 by the hydrothermal method with a mesoporous diameter about 2～7.5 nm.[8] Using the porous SnO_2 as the anode materials for lithium ion battery, the cyclability is much better than that of the pure Sn anode materials, and the coulomb efficiency of first cycle can reach 95%. Uchiyama et al. also obtained a single crystal nano-material of reticular SnO_2 by the hydrothermal method, and the reversible specific capacity of first cycle is about 900 mAh g^{-1}.[9] Although these studies have

prepared TO anode materials with high specific capacity, the process is complex and expensive. Hence, it is urgent to improve the process of TO anode materials for industrial production.

Anodic oxidation can grow oxide film on the anode surface using metal or metal alloy as anode in specific electrolyte. Yang et al. have used ammonium fluoride solution as electrolyte to successfully prepare titania nanotube arrays by anodic oxidation method.[10] Courtney and Dahn found that the voltage platform of 1.58 V of TO anode materials at the first cycle indicates the Li_2O growth in anode because of different Gibbs free energy (Li_2O: 562.1 kJ/mol; SnO_2: 256.8 kJ/mol).[11] And the Li_2O growth is an irreversible process, resulting in the high irreversible capacity in the first cycle. Moreover, since the melting point of tin atom is relatively low, tin atom is easily gathered as clusters, and then two-phase region appears in TO anode materials, leading to the capacity fading during the cycling. Because of above-mentioned problems, scientists have improved TO anode materials by impurity doping.[12-14] Due to the good electrochemical and mechanical performances, CNTs also received wide attention in the field of active materials of lithium-ion battery.[15-18]

In this article, ANSO@CNTs anode material was prepared with composite electrodeposition and anodicoxidation, as shown in Fig. 1. The good electronic conductivity and mechanical properties can be guaranteed by introducing CNTs. The porous structure can facilitate liquid electrolyte diffusion into the active materials. Therefore, it could be expected that the ANSO@CNTs anode material possesses perfect cycling performance and good rate capability.

2. Experimental

2.1. Preparation of CNTs@tin as precursors for anodization

For the electrochemical deposition of CNTs@tin, CNTs should be stirred with PVP (weight

ratio 1:1) for 12 hours, and then the mixture would be added into tin plating solution used as electroplate liquid. A copper sheet was used as the working electrode soaked in degreasers containing caustic soda, natronite, sodium phosphate, and sodium silicate for 5 minutes and diluted sulfuric acid to remove oil contamination and the native surface oxide, respectively, and then cleaned with distilled water. An ordinary tin block is adopted as the counter electrode. A constant cathodic current of 1 A/dm^2 was applied for 5 minutes. The plating tank was under ultrasonic bath conditions with ultrasonic frequency about 45KHz.

2.2. Anodization of CNTs@tin

For the preparation of the ANSO@CNTs anode material, CNTs@tin films in Section 2.1 and graphite flake are used as the working electrode (anode) and the counter electrode (cathode), respectively. The distance between the anode and cathode was kept at 5 cm. A constant potential 8 V was applied to the anode in an electrolyte consisting of 0.1 M oxalic acid at room temperature. An EG&G 263A potentiostat/galvanostat was used in the electrochemical depositions.

2.3. Electrochemical Measurements

The electrochemical experiments have been carried out using the coin cells. The as-prepared samples are cut into wafers used as working electrode. The celgard 2325 microporous membrane was used as the separator. The electrolyte was 1 mol/L $LiPF_6$ dissolved in a mixture of ethylene carbonate (EC) and dimethyl carbonate (DMC) (1:1). The lithium sheet was used as both counter and reference electrode. CR2025-type coin cells were assembled in an argon-filled glove box and galvanostatically discharged and charged in a voltage range from 0.01~2.5 V by a battery testing

system. Cyclic voltammetry (CV) test has been carried out on an electrochemical workstation (Zahner IM6ex) over the potential range 0.01~2.5 V versus Li/Li^+ at a scanning rate of 0.1 mV s^{-1}. Electrochemical impedance spectra of the electrodes were recorded from 1000 KHz~0.1 mHz with the amplitude of 5 mV.

3. Results and discussion

3.1. Microstructural characterization

SEM images of ANSO@CNTs anode material by the one-step anodization in 0.1 M oxalic acid at the potential of 8 V are shown in Figs. 2 (a) and (b). As can be seen, nanopores distribute randomly on the surface with a diameter ranging from about 1 nm to over 20 nm. A dense array of parallel nanochannels, almost perpendicular to the substrate, can be observed obviously. The nanopores structure of tin oxide is similar to the previous investigations.[19, 20] The microstructures and morphologies of the prepared samples are characterized by X-ray diffraction (XRD, Bruker D8 Advance), transmission electron microscopy (TEM, FEI, Tecnai G2 F30 S-Twin), and scanning electron microscopy (Field-Emission SEM, S-4800, Hitachi, Japan), respectively. N_2 adsorption/desorption isotherms were measured using a Micromeritics ASAP 2010 (USA) analyzer at liquid nitrogen temperature. CNTs with a diameter of 10 nm uniformly distribute in the nanoporous SnO layer, as shown in Fig. 2 (c).

Fig. 3 (a) is the XRD spectrum with some peaks of metallic cooper, metallic tin and traces of CNTs. The SnO of as-prepared ANSO@CNTs anode material was found to be amorphous and the dark color of the oxide film suggested formation of SnO during anodization (Fig. 2 (c)). Moreover, the ratio of the Sn atom and O atom was found to be 1:1, corresponding to SnO, and the content of

CNTs is 7.57 Wt%, seen from the EDS map in Fig. 3 (b).

N_2 adsorption-desorption isotherms and pore size distribution of the final ANSO@CNTs anode material are shown in Fig. 4. The nitrogen adsorption-desorption isotherms present obvious pressure hysteresis, indicating that the ANSO@CNTs anode material is porous.[21, 22] The Brunauer-Emmett-Teller (BET) surface area of ANSO@CNTs is 53.4 m^2g^{-1}, and the total pore volume is 0.151 ccg^{-1}. It should be noted that some nanopores smaller than 2 nm exist in the ANSO@CNTs anode material, implying a great benefit to the reversible specific capacity because lithium ion can be stored in these nanopores to further enhance the high rate capability.[23, 24]

3.2. Electrochemical properties of the ANSO@CNTs anode material

The discharge/charge cycles were tested at a specific current of 100 mA g^{-1} by using coin cells, and the 1st, 2nd and 10th discharge/charge curves are shown in Fig. 5 (a). The 1st discharge and charge specific capacities of the ANSO@CNTs anode material are as high as 1895 and 1608 mAh g^{-1}, respectively. The initial coulombic efficiency can reach 85% calculated based on the first discharge/charge specific capacities. The irreversible capacity loss, ~15%, is mainly due to the electrolyte decomposition and the formation of the thick solid-electrolyte interface layer on the electrode surface.[25-27]

Electrochemical behavior of the ANSO@CNTs anode material was well illustrated by the cyclic voltammetry (CV) analysis at a scanning rate of 0.1 mV s^{-1} in Fig. 5 (b). In the reduction process, the hump above 0.5~0.75 V could be attributed to an irreversible separation of SnO to Sn and Li_2O.[28] The peak around 0.3 V reflects the formation of solid-electrolyte interface (SEI) leading to a large irreversible capacity fading, corresponding to the low columbic efficiency in the first

cycle. Meanwhile, in the oxidation process, three peaks were recorded at about 0.6, 0.7 and 0.8 V. The peak at 0.6 V corresponds to lithium extraction from the CNTs [26], and the peak at 0.7 V represents the de-alloying process of Li^+ ions, while the following weak peak at 0.8 V could be ascribed to the reaction of Sn and Li_2O.[29, 30]

Fig. 5 (c) shows the cycle performance and coulombic efficiency during cycling of the ANSO@CNTs anode material. The coulombic efficiency remains near 97%. It can be observed that the cycling stability in the first 22 cycles is not satisfied. From the 2nd cycle, the discharge capacity decreases from 1429.3 mAh g^{-1} to 839.4 mAh g^{-1} after the following 22 cycles and then gradually increases to 890 mAh g^{-1} after 50 cycles. The increasing specific capacity may be due to the formation of an activation process of the ANSO@CNTs. Even at higher current densities of 200, 300, 500, and 1000 mA g^{-1}, the ANSO@CNTs still maintains a perfect cycling stability. After 50 cycles, the discharge capacity is as high as 732.5 mAh g^{-1} at the current density of 100 mA g^{-1}, as shown in Fig. 5 (d). However, the bare ANSO without CNTs doesn't display so well, retaining a charge capacity of 513 mAh g^{-1} after 50 cycles compared to 890 mAh g^{-1} of ANSO@CNTs at the current density of 100 mA g^{-1}. And the ANSO also shows a poor cycling performance in Fig. 5 (c). Therefore, the ANSO@CNTs shows much better charge capacity and cycling performance compared with the bare ANSO, attributed to the good electrochemical and mechanical performances of CNTs in SnO nanoporous layer.

Fig. 6 shows electrochemical impedance spectroscopy of ANSO@CNTs. It can be seen that the ANSO@CNTs anode materials (~59 Ω) has a much lower charge transfer resistance than that of bare ANSO without CNTs (170Ω), indicating a faster Li^+ diffusion and electron transfer in ANSO@CNTs.

4. Conclusions

In summary, ANSO@CNTs was prepared through composite electrodeposition and anodicoxidation. The ANSO@CNTs anode materials exhibits a superior first discharge capacity of 1895 mAh g^{-1} with a reversible capacity of 1608 mAh g^{-1} at the current density of 100 mA g^{-1}. After 40 cycles at different current densities of 100, 200, 500 and 1000 mA g^{-1}, the charge capacity still maintained at 732.5 mAh g^{-1} at the current density of 100 mA g^{-1}. Compared with bare ANSO, the ANSO@CNTs exhibits enhanced Li-ion battery performance with large reversible capacity and good cycling performance. The good electrochemical performances can be attributed to the following reasons: (1) The nanoporous material has high reactivity and short path lengths for electronic and Li^+ transport; (2) Large numbers of mesoporous can provide huge buffer space for volume deformation during the charge-discharge process, improving the cycle performance; (3) Uniform inserted CNTs alleviated chalking of electrode during discharge/charge progress and improved Li^+ transport speed. The ANSO@CNTs can be a promising alternative anode material used for high-storage lithium-ion batteries.

Acknowledgements

We gratefully acknowledge financial support from the National Natural Science Foundation of China (Nos. 11372267 and 11102176), the National High Technology Research and Development Program of China (863 Program) (2013AA032502), and the Emerging Strategic Industries of Hunan Province (2012GK4075).

References

1. J. Cheng, Y. Pan, J. Zhu, Z. Li, J. Pan and Z. Ma, *J. Power Sources*, 2014, **257**, 192-197.
2. Y. Wang, Z. Feng, C. Zhang, L. Yu, C. Shi, J. Chen, J. Hu and X. Liu, *Nanocale*, 2013, **5**, 3704-3712.
3. Y. Wang, Z. Feng, J. Chen, C. Zhang, X. Liu and J. Hu, *Solid State Commun.*, 2012, **152**, 1577-1580.
4. X. Zhou, Z. Dai, S. Liu, J. Bao and Y. G. Guo, *Adv. Mater.*, 2014, **26**, 3943-3949.
5. Y. Idota, T. Kubota, A. Matsufuji, Y. Maekawa and T. Miyasaka, *Science*, 1997, **276**, 1395-1397.
6. M. O. Guler, O. Cevher, T. Cetinkaya, U. Tocoglu and H. Akbulut, *Int. J. Energy Res.*, 2014, **38**, 487-498.
7. Z. Ma, T. Li, Y. Huang, J. Liu, Y. Zhou and D. Xue, *RSC Adv.*, 2013, **3**, 7398-7402.
8. K. Shiva, M. S. R. N. Kiran, U. Ramamurty, S. Asokan and A. Bhattacharyya, *J. Solid State Electrochem.*, 2012, **16**, 3643-3649.
9. H. Uchiyama, S. Nakanishi and H. Kozuka, *J. Solid State Chem.*, 2014, **217**, 87-91.
10. D. J. Yang, H. Park, H. G. Kim, S. J. Cho and W. Y. Choi, *J. Electroceram.*, 2009, **23**, 159-163.
11. I. A. Courtney and J. Dahn, *J. Electrochem. Soc.*, 1997, **144**, 2943-2948.
12. J. S. Chen, L. A. Archer and X. W. D. Lou, *J. Mater. Chem.*, 2011, **21**, 9912-9924.
13. J. S. Chen and X. W. D. Lou, *Small*, 2013, **9**, 1877-1893.
14. S. H. Lee, S. H. Jee, K. S. Lee, S. C. Nam and Y. S. Yoon, *Electrochim. Acta*, 2013, **87**, 905-911.
15. M. Reddy, G. Subba Rao and B. Chowdari, *Chem. Rev.*, 2013, **113**, 5364-5457.

16. H. Song, N. Li, H. Cui and C. Wang, *Electrochim. Acta*, 2014, **120**, 46-51.

17. L. Noerochim, J.-Z. Wang, S.-L. Chou, H.-J. Li and H.-K. Liu, *Electrochim. Acta*, 2010, **56**, 314-320.

18. W. Lei, Y. Pan, Y. Zhou, W. Zhou, M. Peng and Z. Ma, *RSC Adv.*, 2014, **4**, 3233-3237.

19. J. W. Lee, S. J. Park, W. S. Choi and H. C. Shin, *Electrochim. Acta*, 2011, **56**, 5919-5925.

20. L. Zaraska, N. Czopik, M. Bobruk, G. D. Sulka, J. Mech and M. Jaskuła, *Electrochim. Acta*, 2013, **104**, 549-557.

21. S. M. Paek, E. Yoo and I. Honma, *Nano Lett.*, 2008, **9**, 72-75.

22. L. Yu, C. Falco, J. Weber, R. J. White, J. Y. Howe and M. M. Titirici, *Langmuir*, 2012, **28**, 12373-12383.

23. Y. G. Guo, J. S. Hu and L. J. Wan, *Adv. Mater.*, 2008, **20**, 2878-2887.

24. J. Zhu, D. Wang, L. Wang, X. Lang and W. You, *Electrochim. Acta*, 2013, **91**, 323-329.

25. L. Ji, Z. Lin, M. Alcoutlabi and X. Zhang, *Energ. Environ. Sci.*, 2011, **4**, 2682-2699.

26. F. M. Hassan, Z. Chen, A. Yu, Z. Chen and X. Xiao, *Electrochim. Acta*, 2013, **87**, 844-852.

27. P. Abellan, B. L. Mehdi, L. R. Parent, M. Gu, C. Park, W. Xu, Y. Zhang, I. Arslan, J. Zhang and C. Wang, *Nano Lett.*, 2014, **14**, 1293-1299.

28. G. A. Elia, S. Panero, A. Savoini, B. Scrosati and J. Hassoun, *Electrochim. Acta*, 2013, **90**, 690-694.

29. J. Yao, X. Shen, B. Wang, H. Liu and G. Wang, *Electrochem. Commun.*, 2009, **11**, 1849-1852.

30. P. Lian, X. Zhu, S. Liang, Z. Li, W. Yang and H. Wang, *Electrochim. Acta*, 2011, **56**, 4532-4539.

Figure captions

Fig. 1. Schematic representation of the experimental procedure

Fig. 2. SEM images of the ANSO@CNTs anode material: (a) an overview, (b) a zoom part image, and (c) TEM image

Fig. 3. (a) XRD pattern and (b) EDS analysis of the ANSO@CNTs anode material

Fig. 4. (a) Nitrogen adsorption-desorption isotherms of the ANSO@CNTs anode material, (b) Porosity distribution by Original Density Functional Theory Model

Fig. 5. (a) 1st, 2nd and 10th discharge/charge curves at 100 mAg^{-1} of the ANSO@CNTs anode material, (b) Cyclic voltammograms at a scanning rate of 0.1 mVs^{-1} of the ANSO@CNTs anode material, (c) Capacities versus cycle number between 0.01 and 2.5 V at the current density of 100 mAg^{-1} of the ANSO@CNTs and ANSO anode material, (d) Rate capability of the ANSO@CNTs and ANSO anode material

Fig. 6. Electrochemical impedance spectra of (a) ANSO@CNTs anode material and (b) ANSO anode material

Figures

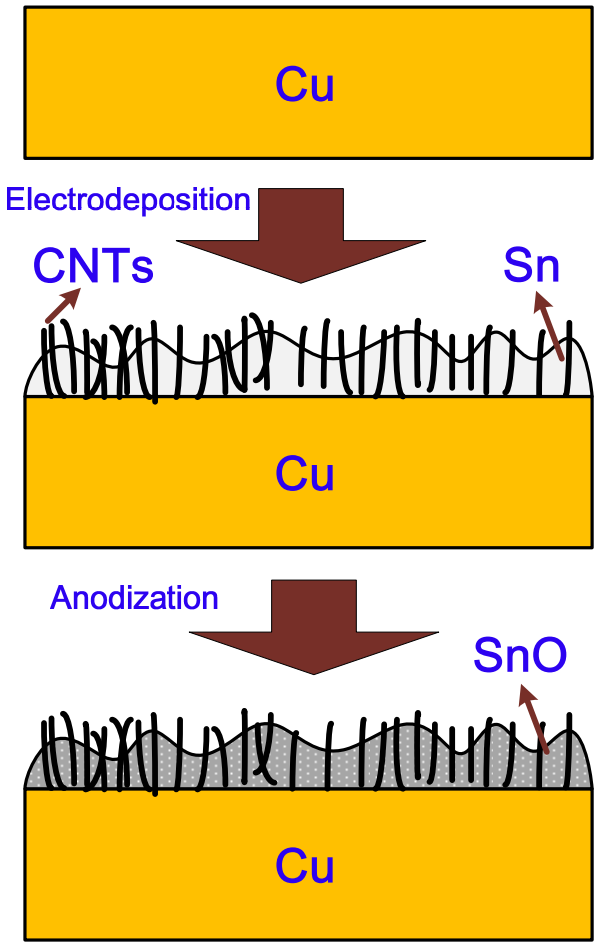

Fig. 1

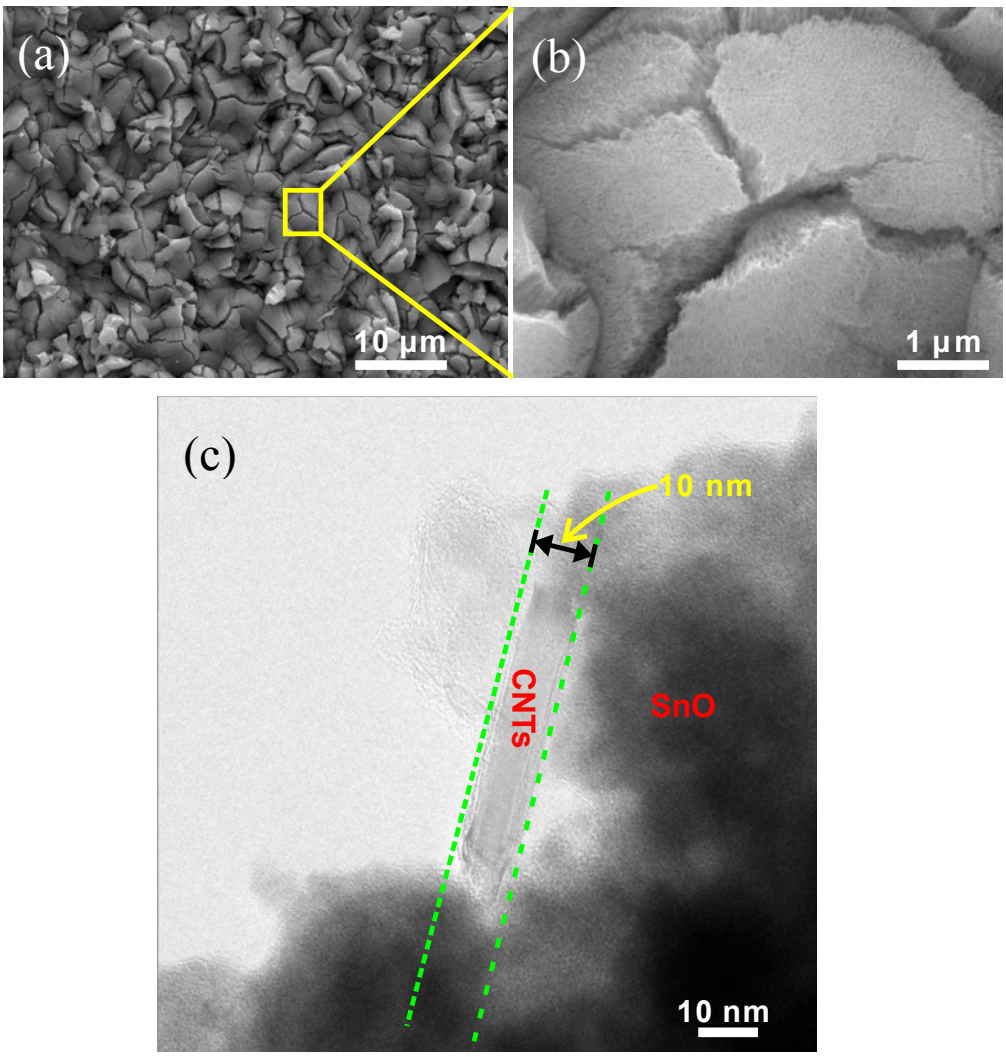

Fig. 2

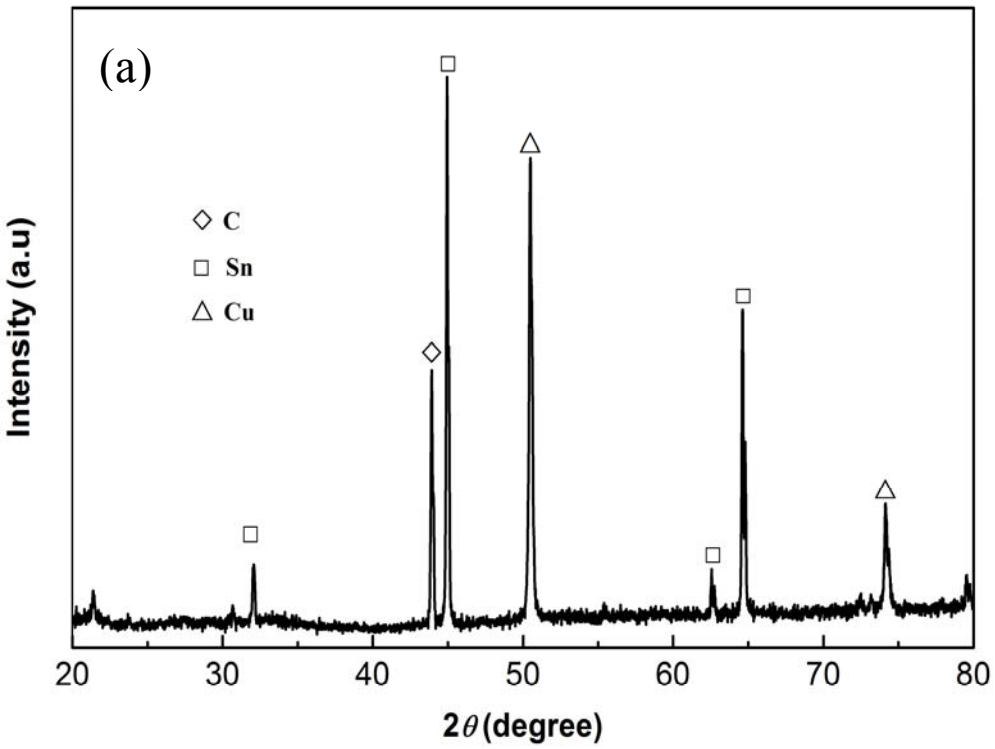

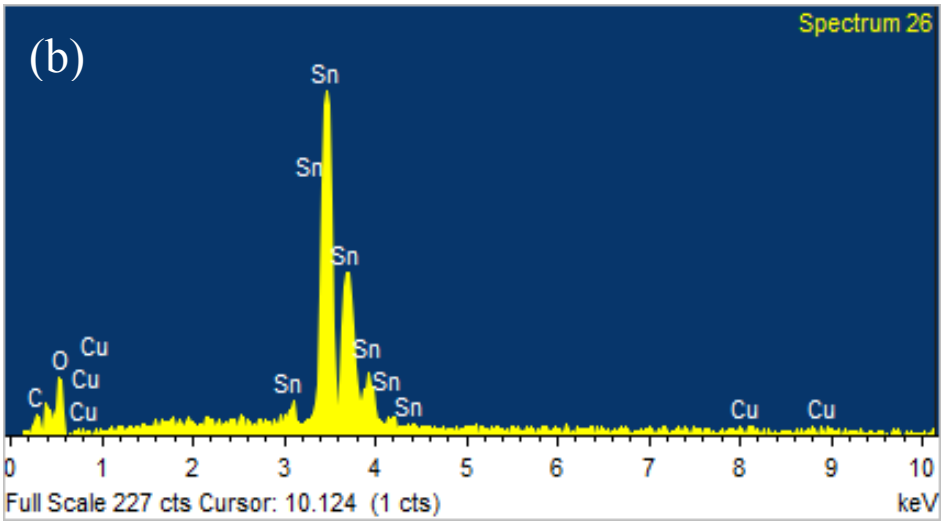

Fig. 3

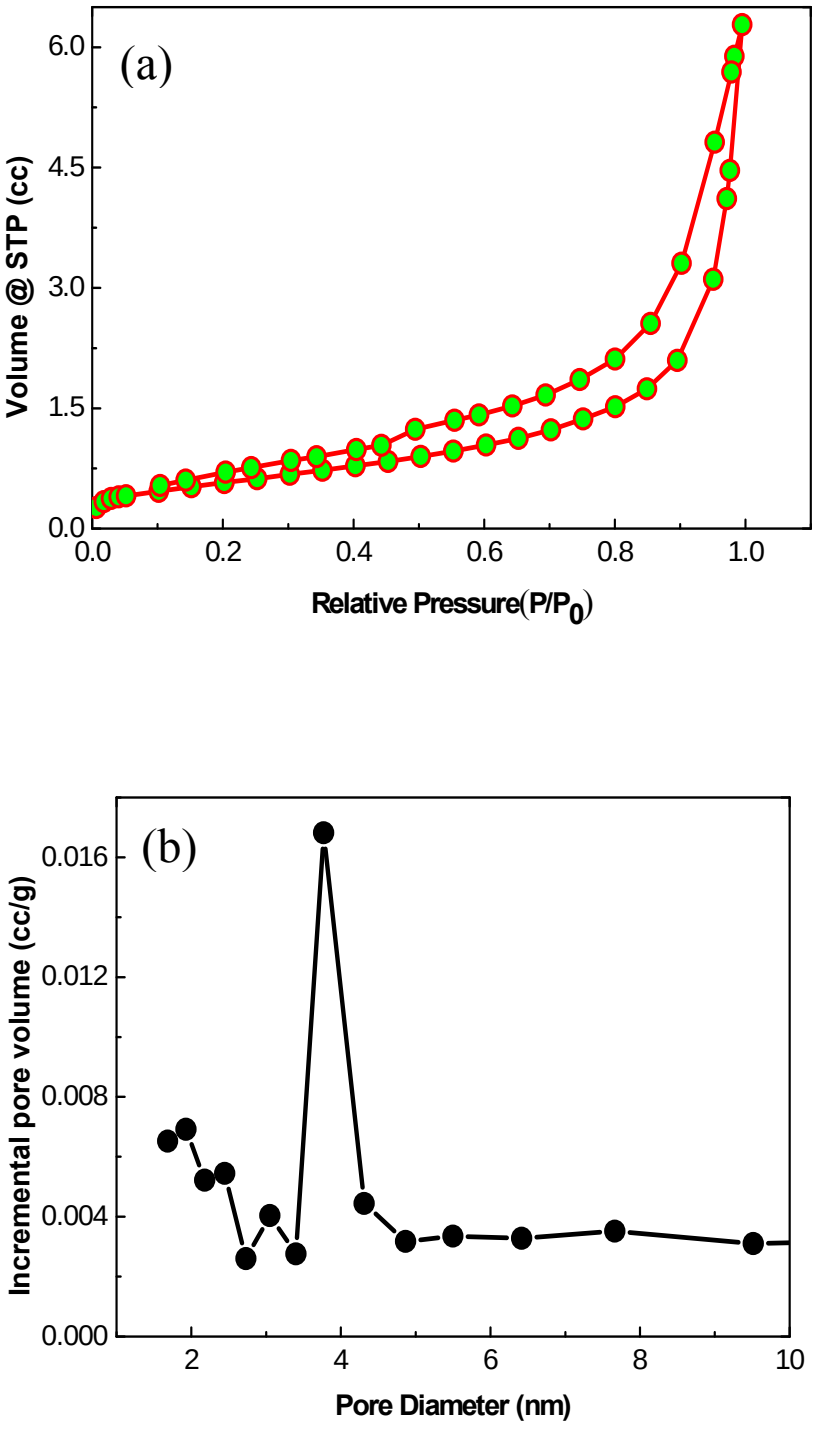

Fig. 4

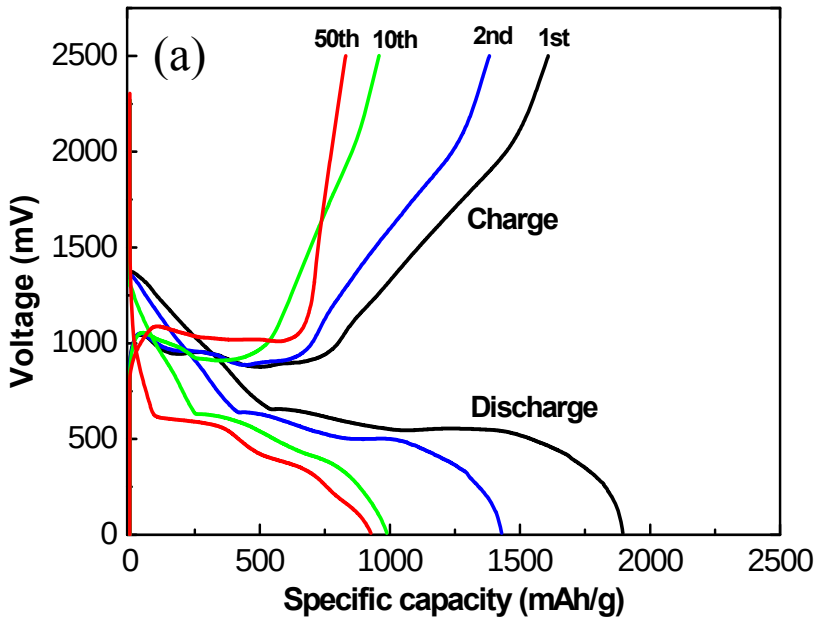

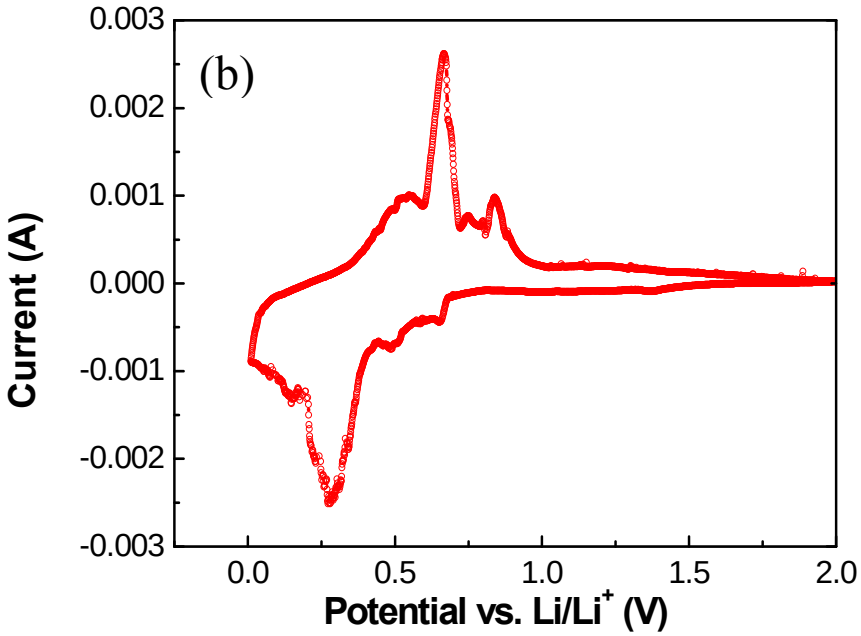

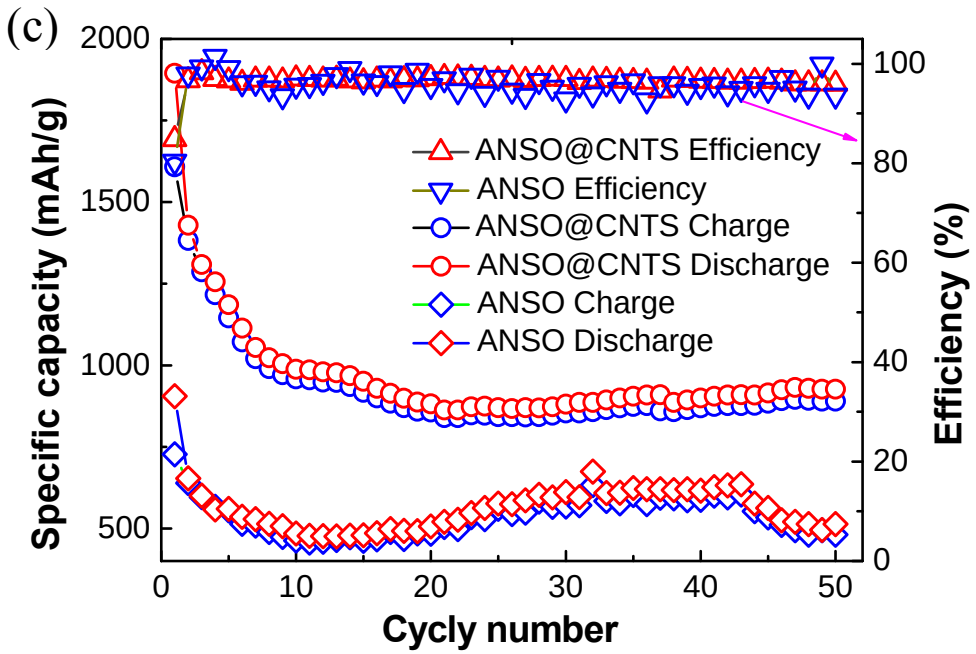

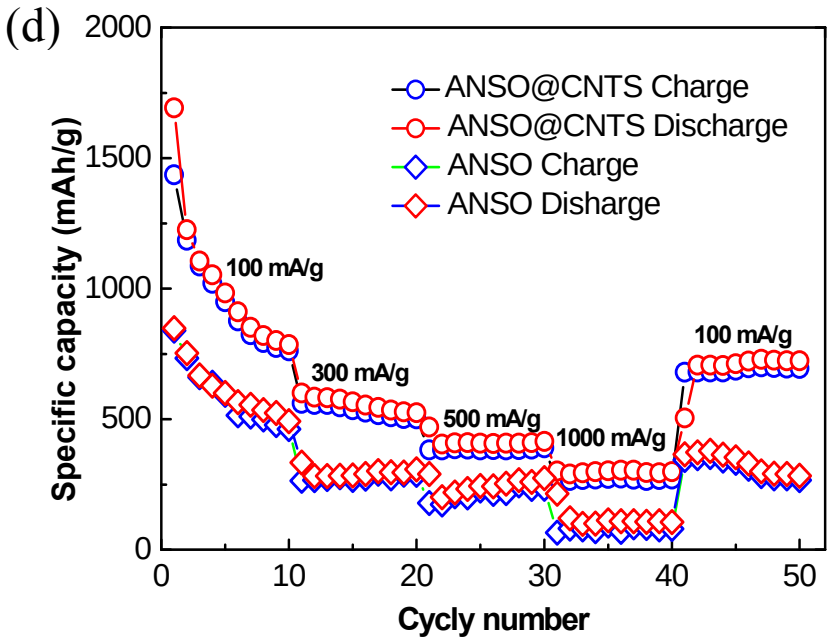

Fig. 5

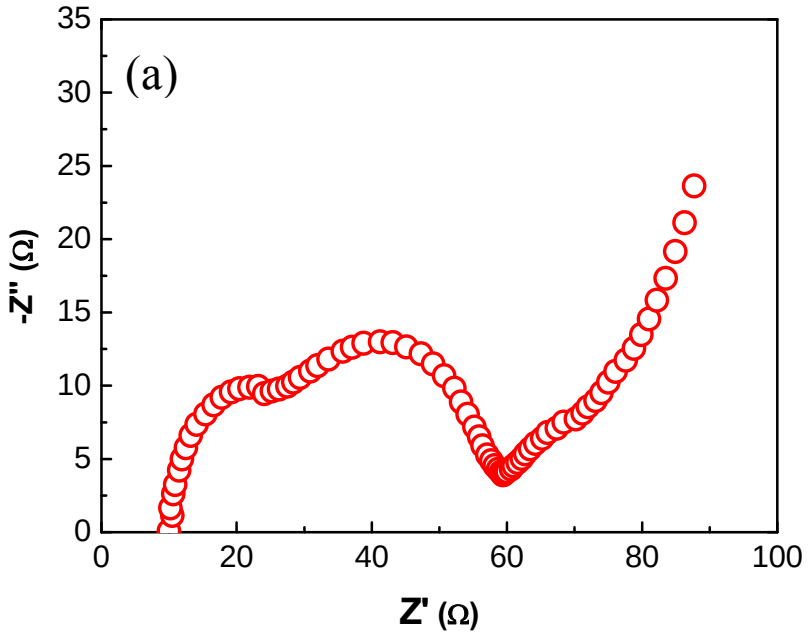

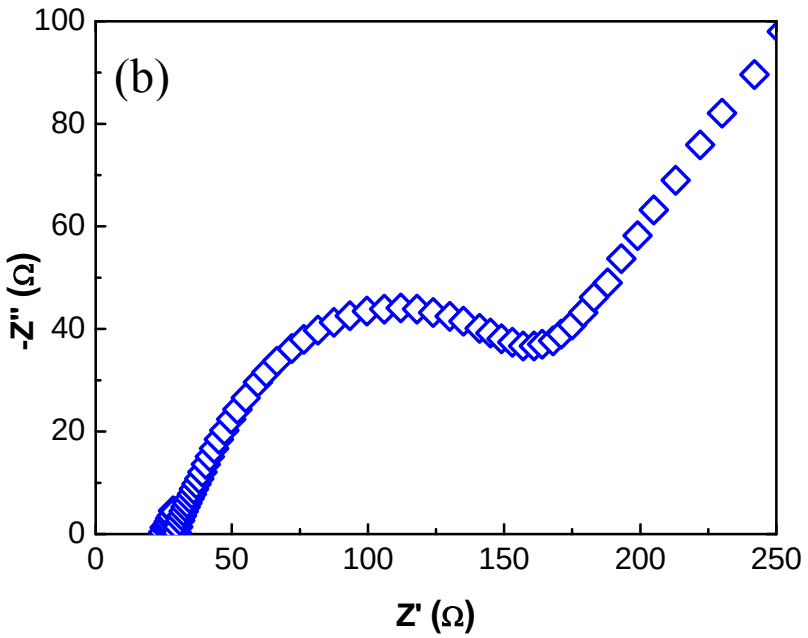

Fig. 6